### Title

Shearing Behavior of Interfaces between Tire-Derived Aggregate and Three Soil Materials




### Journal

Journal of Materials in Civil Engineering, 32(6)

### ISSN

0899-1561



### Authors

Ghaaowd, I

Fox, PJ

McCartney, JS



### Publication Date

2020-06-01

### DOI

10.1061/(asce)mt.1943-5533.0003213

Peer reviewed

# SHEARING BEHAVIOR OF INTERFACES BETWEEN TIRE DERIVED AGGREGATE AND THREE SOIL MATERIALS

**by I. Ghaaowd, Ph.D., S.M.ASCE[1] , P.J. Fox, Ph.D., P.E., F.ASCE[2], and J.S. McCartney, Ph.D., P.E., F.ASCE[3]**

**Abstract:** When tire derived aggregate (TDA) is used as a lightweight monolithic fill in civil engineering applications, such as embankments and retaining walls, the shearing behavior of TDA interfaces with different materials should be carefully considered. This paper presents results from large-scale direct shear tests performed on interfaces between Type B TDA and layers of sand, aggregate, and clay for initial normal stress ranging from 19.0 to 76.7 kPa. To match field conditions, a separation nonwoven geotextile was used at the TDA-sand and TDA-clay interfaces, and a separation woven geotextile was used at the TDA-aggregate interface. Large shear displacements, typically between 200 mm and 350 mm, were required to fully mobilize the secant friction angle. Peak secant interface friction angles range from 26 to 32°, and peak strength envelopes are linear for the sand interface and nonlinear for the aggregate and clay interfaces. Failure envelopes for the TDA-soil interfaces are bounded above by the Type B TDA internal failure envelope and below by the Type B TDA-concrete interface failure envelope. A pair of replicate tests using woven and nonwoven geotextiles for the TDA-aggregate interface indicated that geotextile type had little effect on measured shear behavior as they only provide separation.

[1] Research Associate IV, Louisiana Transportation Research Center, Louisiana State University, 4101 Gourrier Avenue., Baton Rouge, LA 70808; ighaaowd@lsu.edu
[2] Shaw Professor and Head, Department of Civil and Environmental Engineering, Pennsylvania State University, University Park, PA 16802; pjfox@engr.psu.edu
[3] Professor and Department Chair, Dept. of Structural Eng., Univ. of California San Diego, 9500 Gilman Dr., La Jolla, CA 92093-0085; mccartney@ucsd.edu

## INTRODUCTION

Lightweight fills are important materials in highway embankments or retaining walls that are used to minimize settlements of underlying soft subgrade soils. It is well established that shredded waste tires can be used as lightweight construction material for civil engineering applications (Geosyntec 2008; Ahn et al. 2014; CalRecycle 2015). When shredded tires are used alone, without being mixed with soil, the material is referred to as Tire-Derived Aggregate (TDA). The unit weight of compacted TDA is approximately 5 to 9 kN/m$^3$, which is less than one-half of the typical unit weight of granular backfill soils. Many studies have reported projects where TDA was used as a lightweight fill replacement for granular foundation soil in highway embankments or subgrades (Geisler et al. 1989; Ahmed and Lovell 1993; Bosscher et al. 1993, 1997; Hoppe 1998; Dickson et al. 2001; Tandon et al. 2007; Meles et al. 2013), backfill for buried pipes (Mahgoub and El Naggar 2019), material for seismic isolations systems (Tsang 2008; Senetakis et al. 2009), or lightweight fill replacement for granular soil in retaining walls (Humphrey et al. 1992, 1993; Tweedie et al. 1998; Xiao et al. 2012; Ahn et al. 2014). These studies have shown the performance of TDA to be comparable to or better than soil fill materials. ASTM D6270 (ASTM 2017) categorizes TDA by the size range of the shredded tire particles and places limits on the amount of sidewall tire pieces and length of exposed steel wires. According to this standard, Type A TDA has maximum particle size dimensions from 75 to 100 mm and Type B TDA has maximum particle dimensions ranging from 150 to 300 mm. Type B TDA requires less processing than Type A TDA and is therefore more cost-effective for earth fill applications.

Ghaaowd et al. (2017) provided a review of previous experimental studies investigating the shearing behavior of TDA. They found that a relatively large shear device is needed to accommodate the large particles in Type B TDA and that a large horizontal displacement is needed

to fully mobilize the secant friction angle of this material. Although several studies have focused on the internal shearing behavior of TDA, crumb rubber, and soil-shredded tire mixtures, fewer studies have investigated the shearing behavior of TDA interfaces (e.g., Bernal et al. 1997; Xiao et al. 2012; Ghaaowd et al. 2017). Of these studies, only Ghaaowd et al. (2017) provided results on the shearing behavior of Type B TDA interfaces with concrete. Xiao et al. (2012) performed direct shear tests on the interfaces between Type A TDA (maximum particle size = 75 mm) and sand, concrete, a uniaxial geogrid, and a woven geotextile, and reported failure envelopes for these interfaces in terms of friction angles and adhesion values. The adhesion values reported in this study may have resulted from fitting a linear failure envelope to nonlinear data or because the interface frictional resistance was not fully mobilized within the maximum displacement of their device (165 mm). To account for the effects of large particle size in Type B TDA, Fox et al. (2018) developed a large-scale combination shear device to characterize the shearing properties of Type B TDA in either direct shear or simple shear mode. Ghaaowd et al. (2017) used this device to perform internal direct shear tests on Type B TDA and direct shear tests on the interface between Type B TDA and Portland cement concrete. In contrast to the results from Xiao et al. (2012), Ghaaowd et al. (2017) did not observe a drained adhesion value for the TDA-concrete interface. Further, the TDA-concrete interface friction angle of 22.6° reported by Ghaaowd et al. (2017) was much smaller than the value of 35.5° reported by Xiao et al. (2012). This discrepancy in results indicates that additional test data are needed to characterize the interface shearing properties of Type B TDA with different materials.

This study presents a comparison of interface direct shear tests involving Type B TDA and different mineral soils that may be encountered in the construction of embankments or retaining walls. Specifically, this study presents a comparison of tests performed in the large-scale direct

shear box developed by Fox et al. (2018) focused on understanding the shearing behavior of the interfaces between Type B TDA and sand, aggregate base course, and clay interface materials. This large-scale direct shear device is necessary to account for the effects of the large particle size on the shear behavior (i.e., large containers are needed to minimize restriction on movement of partices) and to permit large displacements needed to fully mobilize the frictional resistance at the interface. It is critical to understand the interaction between TDA and different materials as ASTM D6270 restricts the thickness of TDA layers in embankments or retaining walls to 3 m, which means that there will be interaction between TDA layer and mineral soils that are used to separate layers of TDA. Further, TDA will interact with different soils at the base and sides of embankments or retaining walls. and granular aggregate base soil may be placed above a TDA layer to form an overlying roadway, so it is critical to understand the behavior of these TDA interfaces. At the same time, in practice TDA is not placed in direct contact with mineral soils. Instead, a geotextile separation layer is used to provide separation and drainage between the TDA and the given soil. Nonwoven geotextiles are commonly used to separate TDA from clay subgrades or sand backfills, while woven geotextiles are used to separate TDA from overlying granular base course layers. When geotextiles are used in separation applications, they are not expected to provide any tensile resistance to the interface and are solely meant to separate the two materials. They must be included to replicate field conditions but are not expected to provide a mechanical contribution to the shearing behavior.

## MATERIALS

### Type B TDA

Information on the Type B TDA material used in this study is presented in Table 1 and is described in more detail by Ghaaowd et al. (2017). The TDA particles are planar in nature, with

an out-of-plane thickness ranging from 6 to 20 mm. Because the particles have different shapes, their size was defined as the maximum dimension (i.e., length). The TDA in-plane particle size ranges from 30 to 320 mm, with a mean in-plane size $D_{50}$ of 120 mm. A few TDA particles exceeded the in-plane maximum dimension limit of 300 mm set by ASTM D6270. Due to the relatively flat and large dimension of the particles, the measurements in Table 1 required manual identification and sorting of particles by size. A specific gravity of 1.15 was measured for the TDA and used to calculate void ratio from measured dry unit weight in Table 1. This specific gravity value is consistent with the corresponding value of 1.15 for crumb rubber (FHWA 1998) and the typical range of 1.02 to 1.27 for TDA (Bressette 1984; Humphrey et al. 1992; Humphrey and Manion 1992; Ahmed 1993).

## Mineral Soils

Three mineral soils were used in the current testing program and consisted of sand, aggregate, and clay. Particle size distributions for the three soils are shown in Figure 1(a). Based on these relationships, the sand is classified as SW and the aggregate is classified as SP according to the Unified Soil Classification System (USCS). The size gradation for the aggregate is within specification limits for Caltrans Class 2 aggregate base course. The clay consists of a mixture of 60% silty sand and 40% Georgia kaolinite clay by dry weight, with Atterberg limits provided in Figure 1(a), and is classified as CL according to the USCS.

Standard Proctor compaction curves for the three mineral soils are shown in Figure 1(b), along with the zero air voids curve corresponding to a specific gravity of 2.6. The target compaction condition for each soil is also indicated. The aggregate and clay layers investigated in this study were both compacted at their optimum gravimetric water contents and maximum dry unit weights as reflected in Figure 1(b). The compaction curve for the sand was relatively flat, so a low

gravimetric water content of 5% was used for sand compaction to provide good workability, and a target dry unit weight of 18.0 kN/m$^3$ was achieved in all of the tests involving sand. Zheng et al. (2017) reported that the drained internal friction angle for the dry sand is 51.3° for the range of normal stresses in this study. The aggregate has a friction angle of approximately 52° for the low compaction water contents and relative density corresponding to the conditions evaluated in this study (Theyse 2002). Independent shearing tests for the optimal compaction conditions were not performed for the clay soil. However, based on the target dry unit weights shown by the hollow circles in Figure 1(b), it is expected that the aggregate will provide a denser, firmer interface and interact less with the overlying Type B TDA than will the looser, softer sand or clay soils.

## Geotextiles

In engineering practice, a geotextile typically is placed between TDA and soils to provide separation between the materials. Accordingly, a separation geotextile was placed between the TDA and mineral soils for the interface shear tests and the weakest interface was permitted to form during shearing. Based on recommendations from the California Department of Resources Recycling and Recovery (CalRecycle), a nonwoven geotextile (Mirafi 140N) was used at the TDA-sand and TDA-clay interfaces and a woven geotextile (Mirafi 600x) was used at the TDA-aggregate interface. The nonwoven geotextile has a thickness of 1.4 mm and a tensile strength of 0.53 kN, while the woven geotextile has a thickness of 0.6 mm and a grab tensile strength of 0.32 kN. A woven geotextile was used for the TDA-aggregate specimen because this more closely replicates field conditions where aggregate is placed over a TDA fill to form a roadway base course on top of a retaining wall. In this case, the woven geotextile is used both for separation and basal reinforcement. To evaluate the effect of the woven geotextile, an additional shear test was performed using the nonwoven geotextile at the TDA-aggregate interface. A nonwoven geotextile

was used for the sand and clay interfaces to replicate field conditions where a separation geotextile is installed before placing TDA. The separation geotextiles are not restrained in the experiments in these studies and only expected to separate the TDA and soil layers without providing mechanical improvement.

## EXPERIMENTAL PROCEDURES

The experimental program consisted of 11 interface shear tests using Type B TDA and the three mineral soils with separation geotextiles in between, as summarized in Table 2. The tests were conducted using the large-scale combination direct shear/simple shear device developed by Fox et al. (2018) in direct shear mode, with the mineral soils in the lower, stationary shear box and the TDA in the upper, moving shear box. The bottom surface of the lower shear box was covered with plywood to provide a level surface for soil placement. A 1.5 mm-thick smooth geomembrane was placed on the plywood and two layers of 0.75 mm-thick plastic sheeting were placed on the sides of the lower shear box, as shown in Figure 2(a), to reduce the friction between the soil and box, protect the box from corrosion, and prevent loss of water from the compacted soil. Soil lift heights were marked on the plastic sheeting and each ach lift was compacted using five passes of a 60 kg vibratory plate compactor (model vp1135 from Wacker Neuson), as shown in Figure 2(b). Soil compaction conditions were measured using sand cone tests. The achieved dry unit weights of the soil lifts were between 95% and 100% of the target values shown as the hollow circles in Figure 1(b).

After the last soil lift was compacted in the lower shear box, the soil block was leveled [Figure 2(c)], a geotextile was placed on the soil block and temporarily clamped to the lower shear box [Figure 2(d)], the upper shear box was placed and connected to the lower shear box [Figure 2(e)], and the inside walls of the upper shear box were lined with two layers of plastic sheeting. Type B

158 TDA was compacted in 100 mm-thick lifts using a 6 passes of a rolling vibrating compactor with
159 a weight of 14.4 kN, as shown in Figure 2(f). Plywood sheets temporarily were placed against the
160 inside walls of the upper shear box during TDA compaction to avoid damage to the plastic
161 sheeting. The Type B TDA was observed to densify during compaction, indicating a higher unit
162 weight and lower void ratio than loosely-placed TDA. The TDA layer in the upper shear box was
163 compacted in dry conditions to an initial thickness of 889 mm and initial unit weight of 6.3 kN/m$^3$
164 for each shear test. This initial unit weight is expected to be representative of the initial unit weight
165 in the field due to the use of a fully-scale rolling vibrating compactor used in construction
166 applications.

167 To apply normal stress to the test specimen, a rigid top load plate was placed on top of the
168 TDA layer and dead weights were stacked on the plate, as shown in Figure 3(a). Higher normal
169 stresses were applied using a saddle frame (Fox et al. 2018) that allowed additional dead weights
170 to be stacked on the sides of the shear device, as shown in Figure 3(b), which served to lower the
171 center of gravity of the applied load and reduce the potential for tipping instability. Changes in
172 specimen thickness during the application of normal stress and during shear were measured at the
173 four corners of the load plate using linear potentiometers. The normal stress remained on each
174 specimen for a minimum of 12 hours (overnight) prior to shear testing. The final thickness of the
175 TDA layer after the loading period was used to calculate the values of initial unit weight provided
176 in Table 2. Most of the measured settlement occurred due to compression of the TDA material, as
177 the surface of the underlying soil layers did not show visible settlement after shearing.

178 After the loading period was completed, a 20-tonne laboratory crane was used to lift the frame
179 of the upper shear box (i.e., not the TDA material), which was facilitated by the low friction plastic
180 sheeting, and open a 200-mm gap between the upper shear box and the lower shear box. A gap is

necessary because TDA particles aligned perpendicular to the shear plane may provide tensile resistance that may augment the shearing behavior between the TDA and underlying soil, and also to avoid steel-on-steel contact during the entire shearing process. The gap was selected to be greater than the mean particle dimension of the TDA particles (120 mm), and the top and bottom boxes were never observed to touch in any of the tests performed. The rigid top load plate then was fixed to the upper shear box frame so that the entire weight of the top half of the shear box, including the TDA self-weight, frame, and dead weights, was applied as the initial normal stress to the shearing surface, with initial values provided in Table 2. After all displacement sensors were stabilized, the geotextile was unclamped so that shear could occur along the weakest interface, and the test specimen was sheared in air-dry conditions and at a constant horizontal displacement rate of 10 mm/min.

After each shear test was completed, the dead weights and TDA material were removed, and photographs were taken of the geotextile and mineral soil surface. Care was used not to cause TDA particle segregation or lose smaller TDA particles during handling, as the same TDA material was used for all shear tests. For a subsequent test using the same mineral soil type, the top two lifts of the soil layer were removed and recompacted to construct the next test specimen. For the TDA-aggregate tests, tell-tales were attached to the end of the geotextile to monitor relative movement between the geotextile and soil layer during shear to compare the behavior between tests with nonwoven and woven separation geotextiles. As will be noted, negligible displacements were noted for the nonwoven geotextile in these tests, so tell-tales were not included on the nonwoven geotextiles in the experiments on the other interfaces. At the same time, post-tests observations indicate negligible displacements for the nonwoven geotextiles in the other tests confirming that they were not necessary.

# RESULTS

## TDA Unit Weights

An evaluation of the initial unit weights of the TDA layers in each of the experiments immediately before shearing is shown in Figure 4, along with the initial unit weights of the TDA in the internal direct shear and TDA-concrete direct shear tests reported by Ghaaowd et al. (2017). This figure represents the compression of the TDA layer after loading to different normal stresses while overlying different interfaces. Although there are some variations in the initial unit weight of the TDA in the interface direct shear tests, generally less compression is observed with increasing vertical normal stress at the location of the shearing plane. This may be related to slightly different TDA unit weights achieved by compaction in the different tests (i.e., the unit weight before application of the vertical normal stress) but may also be related to the differences in thickness of the TDA layers investigated in the internal and interface tests. The normal stresses in Figure 4 denoted as initial values as the normal stress will increase during shear due to the decrease in contact area.

## TDA-Sand Interface Shearing Tests

Experimental results for three direct shear tests on the Type B TDA-sand interface with a separation nonwoven geotextile and initial normal stress ranging from $\sigma_{n,0}$ = 38.8 to $\sigma_{n,0}$ = 76.7 kPa are presented in Figure 5. As discussed by Ghaaowd et al. (2017), the area of the shearing surface decreases during shear displacement $\delta$, which has the effect of steadily increasing the normal stress $\sigma_n$ and shear stress $\tau$ at the interface. Area-corrected relationships for shear stress versus shear displacement are shown in Figure 5(a). For each normal stress, shear stress increases rapidly with shear displacement at the beginning of the test and then gradually increases to the displacement limit of the shear device (approx. 1 m). The data in Figure 5(a) do not show a peak shear stress

because normal stress increases during shear. Corresponding relationships for mobilized secant friction angle $\phi_{sec}$ [= arctan ($\tau/\sigma_n$)] are shown in Figure 5(b) and indicate close agreement throughout the shearing process. The highest value of $\phi_{sec}$ corresponds to full mobilization of friction and is used to define the conditions representing failure. The peak shear stress at failure $\tau_f$ occurred at shear displacement ranging from 320 mm to 350 mm and the peak secant friction angle decreased slightly with increasing normal stress, from $\phi_{sec,f}$ = 32.0° at $\sigma_{n,0}$ = 38.8 kPa to $\phi_{sec,f}$ = 30.9° at $\sigma_{n,0}$ = 76.7 kPa (Table 2). Shear displacements at failure for the TDA-sand interface generally are smaller than displacements at failure measured for the same Type B TDA material (Ghaaowd et al. 2017). Relationships for volumetric strain versus shear displacement are shown in Figure 5(c) and indicate consistent contraction behavior during shear. Although a negligible effect of normal stress on the volumetric strain was observed when comparing the three tests at different normal stresses, different trends with displacement were observed in each test. Ghaaowd et al. (2017) observed that greater volumetric contraction was observed for higher initial normal stresses. The differences in this study may be due to the thinner TDA layer in the interface tests and the fact that a shear plane formed at the base of the TDA layer (at the interface) instead of within the TDA.

## TDA-Aggregate Interface Shearing Tests

Experimental results for four direct shear tests on the Type B TDA-aggregate interface with a separation woven geotextile and initial normal stress ranging from 19.0 to 49.3 kPa are presented in Figure 6. Results also are presented for an additional replicate test performed using a separation nonwoven geotextile at $\sigma_{n,0}$ = 24 kPa. Area-corrected relationships for shear stress versus shear displacement are shown in Figure 6(a). Similar to the results in Figure 6(a), the relationships show increasing shear stress with no peak value. Interestingly, results for the two tests conducted at

$\sigma_{n,0}$ = 24 kPa are similar and indicate that the separation geotextile type had little effect on interface shear behavior. Instead the geotextiles only served to separate the two materials without providing mechanical effects on the shearing behavior. Corresponding relationships for mobilized secant friction angle are shown in Figure 6(b) and indicate peak strength at shear displacements ranging from 145 to 327 mm. For the woven geotextile specimens, peak secant friction angle generally decreased with increasing normal stress, from $\phi_{sec,f}$ = 33.0° at $\sigma_{n,0}$ = 19.0 kPa to $\phi_{sec,f}$ = 27.3° at $\sigma_{n,0}$ = 49.3 kPa. The nonwoven geotextile specimen yielded $\phi_{sec,f}$ = 31.9°, which is consistent with $\phi_{sec,f}$ = 31.2° measured for the corresponding woven geotextile specimen at $\sigma_{n,0}$ = 24.0 kPa. Relationships for volumetric strain versus shear displacement are shown in Figure 6(c) and indicate increasing contraction behavior with increasing normal stress. The specimen with a nonwoven separation geotextile experienced higher contraction during shear than the corresponding specimen with a woven separation geotextile, but this was likely due to the slightly lower initial TDA unit weight for the test with a nonwoven separation geotextile

Displacements of tell-tales attached to the end of separation geotextiles for the TDA-aggregate tests are presented in Figure 7. The data indicate high relative displacements between the woven geotextiles and the underlying aggregate layer for low normal stress, lower displacements for the woven geotextiles at high normal stress, and essentially no displacement for the nonwoven geotextile during shear. This suggests that the nonwoven geotextile-aggregate interface had higher shear strength than the woven geotextile-aggregate interface. Interestingly, significant differences in relative displacement of separation geotextiles between the aggregate and nonwoven or woven for $\sigma_{n,0}$ = 24.0 kPa did not significantly affect the shearing behavior between the TDA and the aggregate base course.

## TDA-Clay Interface Shearing Tests

Experimental results for three direct shear tests on the Type B TDA-clay interface with a separation nonwoven geotextile and initial normal stress ranging from $\sigma_{n,0}$ = 38.3 to $\sigma_{n,0}$ = 86.1 kPa are presented in Figure 8. Area-corrected relationships for shear stress versus shear displacement are shown in Figure 8(a) and again indicate no peak values. Corresponding relationships for mobilized secant friction angle are shown in Figure 8(b) and, similar to the results in Figure 5(b), indicate close agreement throughout the shearing process and decreasing peak secant friction angles with increasing normal stress, from $\phi_{sec,f}$ = 31.4° at $\sigma_{n,0}$ = 38.3 kPa to $\phi_{sec,f}$ = 29.2° at $\sigma_{n,0}$ = 76.7 kPa. The TDA-clay interfaces display the greatest post-peak strength reduction for the three mineral soil interfaces tested in the current study. Relationships for volumetric strain versus shear displacement are shown in Figure 8(c) and, similar to the results in Figure 5(c), indicate consistent contraction behavior during shear, with relatively small effect of normal stress.

## Final Interface Photographs

Final interface photographs for the highest normal stress tests (i.e., $\sigma_{n,0}$ = 49.3 kPa for aggregate, $\sigma_{n,0}$ = 76.7 kPa for sand, and $\sigma_{n,0}$ = 76.7 kPa for clay) are shown in Figure 9. Although some steel wires protruded into the geotextiles, no tearing of the geotextiles was observed. The surfaces of the sand and clay layers showed indentations from the overlying large TDA particles, whereas the surfaces of the aggregate layers were relatively smooth. The indentations from the overlying large TDA particles in the sand and clay layers indicate that the TDA was still able to engage with the underlying soil layers despite the presence of the geotextiles. Interesting, the woven geotextile produced sliding on the aggregate surface (Fig. 8) and associated differences in shear behavior, which are manifested as a stronger influence of normal stress on both the secant friction angle and volumetric strain relationships.

## FAILURE ENVELOPES

The values of shear stress and normal stress at failure for the three Type B TDA interfaces are shown in Figure 10. The values of shear stress and normal stress at failure were defined as those at the displacement corresponding to the peak mobilized secant friction angle, following the approach described by Ghaaowd et al. (2017). This failure criterion was used to identify the conditions were the interface friction was fully mobilized and must be used because the normal stress varies during shearing due to changes in area. The shear stresses at failure from Type B TDA internal tests and Type B TDA-concrete interface tests reported by Ghaaowd et al. (2017) are also shown for comparison in Figure 10. In general, the shear stresses at failure from the TDA-mineral soil interface tests (current study) lie between the shear stresses at failure from TDA internal tests (highest) and TDA-concrete interface tests (lowest). The shear stresses at failure from the TDA-sand and TDA-clay interface tests are similar, with slightly greater values for TDA-sand at the higher normal stresses. The shear stresses at failure from the TDA-aggregate interface tests are lower those from the TDA-sand and TDA-clay interface tests but are higher than those from the TDA-concrete interface tests. These trends suggest that soils with higher compliance, such as the sand and clay layers in the current study as indicated by indentations on the final shearing surface (Fig. 8), will yield a stronger interface with shear stresses at failure that are closer to those from TDA internal tests.

As the shear stresses at failure for some of the interfaces exhibit a nonlinear trend with the normal stress at failure, the nonlinear failure envelope equation proposed by Duncan et al. (1980) was fitted to the data. The nonlinear failure envelope of Duncan et al. (1980) incorporates a secant friction angle $\phi_{\text{sec,f}}$ that varies with the normal stress at failure, and is given as follows:

$$\tau_f = \sigma_{n,f} tan\left(\phi_{sec,f}\right) \quad (2)$$

where $\tau_f$ and $\sigma_{n,f}$ are the shear stress and normal stress at failure, and $\phi_{\text{sec,f}}$ is defined as:

$$\phi_{sec,f} = \phi_0 + \Delta\phi log\left({}^{\sigma_{n,f}}/_{p_{atm}}\right) \quad (3)$$

where $p_{\text{atm}}$ is atmospheric pressure (101.3 kPa) and $\phi_0$ and $\Delta\phi$ are fitting parameters. Values of $\Delta\phi = 0$ and $\Delta\phi < 0$ correspond to linear and nonlinear failure envelopes, respectively. Parameters for the failure envelopes shown in Figure 10 are summarized in Table 3. The TDA-sand and TDA-concrete interfaces yielded linear envelopes, and the TDA internal and TDA-aggregate and TDA-clay interfaces yielded nonlinear envelopes. The nonlinearity of the TDA-aggregate interface envelope was similar to that of the TDA internal envelope. The TDA-clay interface envelope was slightly nonlinear but similar to the linear TDA-sand failure envelope, except at high normal stress. Zero adhesion was assumed when fitting both the linear and nonlinear failure envelopes as there is no cementation or bonding between the TDA and the underlying soil material. Adhesion is only expected in interface shearing experiments when there is cementation or bonding connection.

## CONCLUSIONS

This paper presents results from 11 large-scale direct shear tests performed on interfaces between Type B TDA and layers of sand, aggregate, and clay for initial normal stresses ranging from 19.0 to 76.7 kPa. Similar to field construction practice, a separation nonwoven geotextile was used at the TDA-sand and TDA-clay interfaces, and a separation woven geotextile was used at the TDA-aggregate interface. Large shear displacements, typically between 200 mm and 350 mm, were required to mobilize the peak secant interface friction angle. Peak secant interface friction angles range from 26° to 32°, and peak strength envelopes are linear for the sand interface and nonlinear for the aggregate and clay interfaces. Failure envelopes for the TDA-soil interfaces are bounded from above by that of the internal Type B TDA and below by that of the Type B TDA-concrete interface. A pair of replicate tests using woven and nonwoven geotextiles for the TDA-

aggregate interface indicated that separation geotextile type had little effect on measured shear behavior as the geotextiles only serve a separation purpose. Finally, no damage was observed to the separation geotextiles for any of the direct shear tests.

## DATA AVAILABILITY

All data and models generated and used during the study appear in the submitted article.

## ACKNOWLEDGMENTS

The authors thank the Powell Laboratory staff in the Department of Structural Engineering at the University of California-San Diego for assistance with the experimental program. Financial support from California Department of Resources Recycling and Recovery (CalRecycle) is gratefully acknowledged. The assistance and support of Stacey Patenaude and Bob Fujii of CalRecycle as well as Joaquin Wright and Chris Trumbull of GHD is also gratefully acknowledged. The contents of this paper reflect the views of the authors and do not necessarily reflect the views of the sponsor.

## REFERENCES

Ahmed, I., and Lovell, C.W. (1993). "Rubber soils as lightweight geomaterials." Transp. Res. Rec., 1422, 61–70.

Ahn, I., Cheng, L., Fox, P.J., Wright, J., Patenaude, S., and Fujii, B. (2014). "Material properties of large-size tire derived aggregate for civil engineering applications." Journal of Materials in Civil Engineering, DOI: 10.1061/(ASCE)MT.1943-5533.0001225, 04014258.

ASTM D6270. (2017) Standard Practice for Use of Scrap Tires in Civil Engineering Applications. ASTM International, West Conshohocken, PA.

360 Bosscher, P.J., Edil, T.B., and Eldin, N. (1993). "Construction and performance of shredded waste
361 tire test embankment." Transportation Research Record. Transportation Research Board,
362 Washington, DC. Volume 1345, 44-52.
363 Bosscher, P.J., Edil, T.B., and Kuraoka, S. (1997). "Design of highway embankments using tire
364 chips." J. of Geotech. and Geoenv. Eng. 123(4), 295-304.
365 Bressette, T. (1984). Used Tire Material as an Alternate Permeable Aggregate. State of California,
366 Department of Transportation, Division of Engineering Services, Office of Transportation
367 Laboratory, Sacramento, CA.
368 CalRecycle. (2010). "Tire Management Overview." <http://www.calrecycle.ca.gov/Tires/
369 Overview.htm> (Accessed on: 1/26/2016).
370 Dickson, T.H., Dwyer, D.F., Humphrey, D.N. (2001). "Prototype tire-shred embankment
371 construction." Transportation Research Record. 1755, 160-167.
372 Duncan, J.M., Byrne, P., Wong, K.S. and Mabry, P. (1980). Strength, Stress-strain and Bulk
373 Modulus Parameters for Finite Element Analysis of Stresses and Movements in Soil Masses.
374 Report No. UCB/GT/80-01, Dept. Civil Engineering, U.C. Berkeley.
375 Edil, T.B. and Bosscher, P.J. (1994). "Engineering properties of tire chips and soil mixtures."
376 ASTM Geotechnical Testing Journal. 17(4), 453-464.
377 FHWA (Federal Highway Administration). (1998). "User guidelines for waste and byproduct
378 materials in pavement construction." FHWARD-97-148, U.S. Dept. of Transportation,
379 Washington, DC.
380 Fox, P.J., Thielmann, S.S., Sanders, M.J., Latham, C., Ghaaowd, I., and McCartney, J. S. (2018).
381 "Large-scale combination direct shear/simple shear device for tire-derived aggregate." ASTM
382 Geotechnical Testing Journal. 41(2), 340-353.

Geisler, E., Cody, W.K., and Niemi, M.K. (1989). "Tires for subgrade support." Annual Conf. on Forest Engineering, Council on Fire Engineering. Corvallis. OR, 1–5.

Geosyntec. (2008). Guidance Manual for Engineering Uses of Scrap Tires. Prepared for Maryland Department of the Environment. Geosyntec Project No.: ME0012-11.

Ghaaowd, I., McCartney, J.S., Thielmann, S., Sanders, M. and Fox, P.J. (2017). "Shearing behavior of tire derived aggregate with large particle sizes. I: Internal and concrete interface direct shear behavior." J. of Geotech. and Geoenv. Eng. 143(10), 04017078.

Hoppe, E.J. (1998). "Field study of shredded-tire embankment," Transportation Research Record No. 1619, Transportation Research Board, Washington, DC. 47-54.

Humphrey, D.N., Sandford, T.C., Cribbs, M.M., Gharegrat, H., and Manion, W.P. (1992). Tire Chips as Lightweight Backfill for Retaining Walls - Phase I. Report to the New England Consortium, 137 pp.

Humphrey, D., Sandford, T., Cribbs, M., and Manion, W. (1993). "Shear strength and compressibility of tire chips for use as retaining wall backfill." Transportation Research Record. Transportation Research Board, Washington, DC. Volume 1422, 29–35.

Lee, J.H., Salgado, R., Bernal, A., and Lovell, C.W. (1999). "Shredded tires and rubber-sand as lightweight backfill." J. of Geotech. and Geoenv. Eng. 125(2), 132–141.

Mahgoub, A. and El Naggar, H. (2019). "Using TDA as an engineered stress-reduction fill over preexisting buried pipes." Journal of Pipeline Systems Engineering and Practice. 10(1), 04018034.

Meles, D., Bayat, A., Shafiee, M.H., Nassiri, S. and Gul, M. (2013). "Field study on construction of highway embankment made from two tire derived aggregate types and tire-derived

405 aggregate mixed with soil as fill materials." In Transportation Research Board, 92 Annual
406 Meeting. Washington, DC.

407 Senetakis, K., Anastasiadis, A., Trevlopoulos, K, Pitilakis, K. (2009). "Dynamic response of
408 SDOF systems on soil replaced with sand/rubber mixture." Proceedings of the ECOMAS
409 thematic conference on computation methods in structural dynamics and earthquake
410 engineering. 22-24.

411 Tandon, V., Velazco, D.A., Nazarian, S., and Picornell, M. (2007). "Performance monitoring of
412 embankments containing tire chips: Case study." J. of Perf. of Const. Fac. 21(3), 207–214.

413 Theyse, H.L. (20020). Stiffness, Strength, and Performance of Unbound Aggregate Material:
414 Application of South African HVS and Laboratory Results to California Flexible Pavements.
415 Report to University of California Pavement Research Center. Davis, CA. 1-86.

416 Tsang, H.H. (2008). "Seismic isolation by rubber–soil mixtures for developing countries."
417 Earthquake Engineering and Structural Dynamics. 37(2), 283–303.

418 Tweedie, J.J., Humphrey, D.N., and Sandford, T.C. (1998). "Tire shreds as retaining wall backfill,
419 active conditions." J. of Geotech. and Geoenv. Eng. ASCE, 124(11), 1061-1070.

420 Xiao, M., Bowen, J., Graham, M., and Larralde, J. (2012). "Comparison of seismic responses of
421 geosynthetically-reinforced walls with tire-derived aggregates and granular backfills." J.
422 Mater. Civil Eng., 10.1061 /(ASCE)MT.1943-5533.0000514, 1368–1377.

423 Xiao, M., Ledezma, M., and Hartman, C. (2013). "Shear resistance of tire-derived aggregate using
424 large-scale direct shear tests. Journal of Materials in Civil Engineering. 27(1), 04014110-1-8.

425 Zheng, Y., Sander, A.C., Rong, W., Fox, P.J., Shing, P.B., and McCartney, J.S. (2017). "Shaking
426 table test of a half-scale geosynthetic-reinforced soil bridge abutment." ASTM Geotechnical
427 Testing Journal. 41(1), 171-192.

428 **Table 1.** Particle size information for Type B TDA material

| Parameter | Value |
|---|---|
| Range of particle size | 30-320 mm |
| Range of particle thickness | 6-20 mm |
| $D_{10}$* | 70 mm |
| $D_{30}$* | 105 mm |
| $D_{50}$* | 120 mm |
| $D_{60}$* | 155 mm |
| Coefficient of curvature, $C_c$ | 1.02 |
| Coefficient of uniformity, $C_u$ | 2.21 |

429 *$D_{10}$, $D_{30}$, $D_{50}$, and $D_{60}$ are the largest TDA particle dimension at 10%, 30%, 50%, and 60% finer
430 by dry weight.
431
432

433 **Table 2.** Summary of TDA-sand interface direct shear testing program

| Test Number* | Initial TDA Unit Weight, $\gamma_{d,0}$ (kN/m$^3$) | Initial Normal Stress, $\sigma_{n,0}$ (kPa) | Initial Void Ratio | Displacement Rate (mm/min) | Values at Peak Secant Friction Angle | | | |
|---|---|---|---|---|---|---|---|---|
| | | | | | $\sigma_{n,f}$ (kPa) | $\tau_f$ (kPa) | $\phi_{sec,f}$ (deg) | $\delta_f$ (mm) |
| TDA-NWGT-Sand 1 | 7.20 | 38.8 | 0.57 | 10 | 43.3 | 27.1 | 32.0 | 323.5 |
| TDA-NWGT-Sand 2 | 7.40 | 58.7 | 0.51 | 10 | 66.2 | 40.3 | 31.3 | 349.6 |
| TDA-NWGT-Sand 3 | 8.00 | 76.7 | 0.41 | 10 | 86.4 | 51.7 | 30.9 | 345.0 |
| TDA-WGT-Aggregate 1 | 6.46 | 19.0 | 0.75 | 10 | 20.8 | 13.5 | 33.0 | 259.9 |
| TDA-WGT-Aggregate 2 | 6.98 | 24.0 | 0.71 | 10 | 26.8 | 16.3 | 31.2 | 326.8 |
| TDA-WGT-Aggregate 3 | 7.01 | 33.7 | 0.61 | 10 | 35.4 | 17.8 | 26.7 | 145.3 |
| TDA-WGT-Aggregate 4 | 7.35 | 49.3 | 0.53 | 10 | 53.2 | 27.5 | 27.3 | 229.7 |
| TDA-NWGT-Aggregate 5 | 6.61 | 24.0 | 0.71 | 10 | 26.1 | 16.2 | 31.9 | 260.1 |
| TDA-WGT-Clay 1 | 6.97 | 38.3 | 0.62 | 10 | 41.9 | 25.5 | 31.4 | 263.1 |
| TDA-WGT-Clay 2 | 7.50 | 58.9 | 0.50 | 10 | 64.2 | 36.9 | 29.9 | 250.7 |
| TDA-WGT-Clay 3 | 8.00 | 76.7 | 0.41 | 10 | 86.1 | 48.1 | 29.2 | 335.4 |

434 *NWGT = nonwoven geotextile; WGT = woven geotextile
435

436 **Table 3.** Parameters for TDA failure envelopes.

| Interface | Failure Envelope Parameters | |
|---|---|---|
| | $\phi_0$ (degrees) | $\Delta\phi$ (degrees) |
| Internal TDA (Ghaaowd et al. 2017 | 30.2 | -14.4 |
| TDA-Concrete (Ghaaowd et al. 2017) | 22.6 | 0 |
| TDA-NWGT-Sand | 31.3 | 0 |
| TDA-NWGT-Aggregate | 23.4 | -13.9 |
| TDA-NWGT-Clay | 28.7 | -6.95 |

437
438

## LIST OF FIGURE CAPTIONS

**Figure 1.** (a) Particle size distributions of the soil materials and TDA; (b) Standard Proctor compaction curves for the soil materials

**Figure 2.** (a) Schematic of the direct shear device in interface shear mode; (b) Plastic sheeting attached to side walls of the bottom shear box; (c) Soil compaction using target lift height markers; (d) Surface leveling at the interface; (e) Placement of separation geotextile; (f) Placement of top shear box; (f) TDA compaction in top shear box

**Figure 3.** (a) Direct shear device after loading and lifting of the top box to form a gap under low normal stress; (b) Direct shear device under high normal stress

**Figure 4.** TDA unit weights versus the normal stress at the location of the shearing plane for different TDA interfaces before the start of shearing.

**Figure 5.** TDA-sand interface results: (a) Shear stress-displacement; (b) Mobilized secant friction angle; (c) Volumetric strain

**Figure 6.** TDA-aggregate interface results: (a) Shear stress-displacement; (b) Mobilized secant friction angle; (c) Volumetric strain

**Figure 7.** Displacements of tell-tales attached to the interface geotextile in the tests on the TDA-aggregate specimens.

**Figure 8:** TDA-clay interface results: (a) Shear stress-displacement; (b) Mobilized secant friction angle; (c) Volumetric strain

**Figure 9.** Lower shear box specimens after shearing at highest normal stress: (a) Nonwoven geotextile over sand; (b) Sand surface; (c) Woven geotextile over aggregate; (d) Aggregate surface; (e) Nonwoven geotextile over clay; (f) Clay surface.

**Figure 10.** Failure envelopes for Type B TDA and Type B TDA interfaces

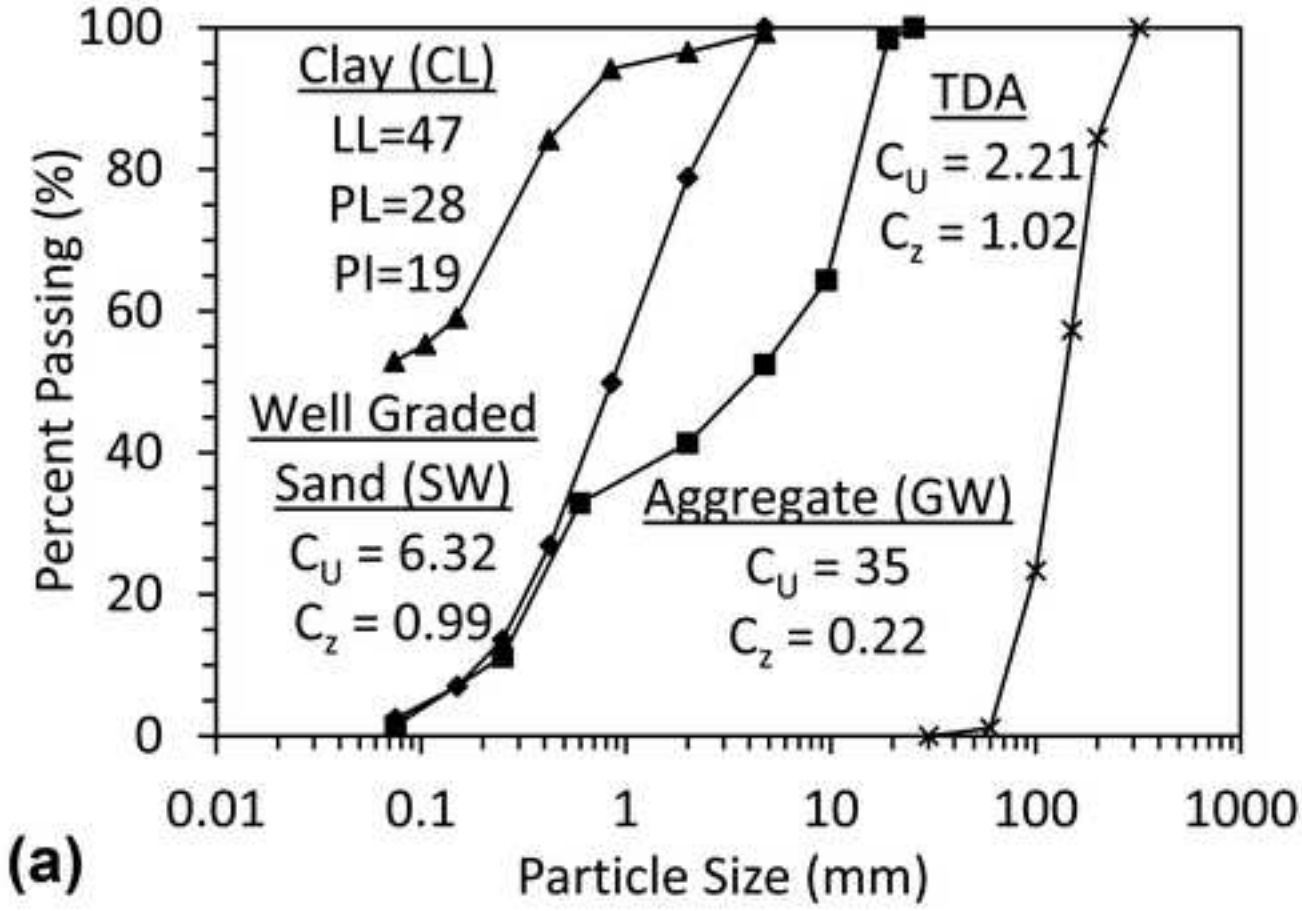


(a)

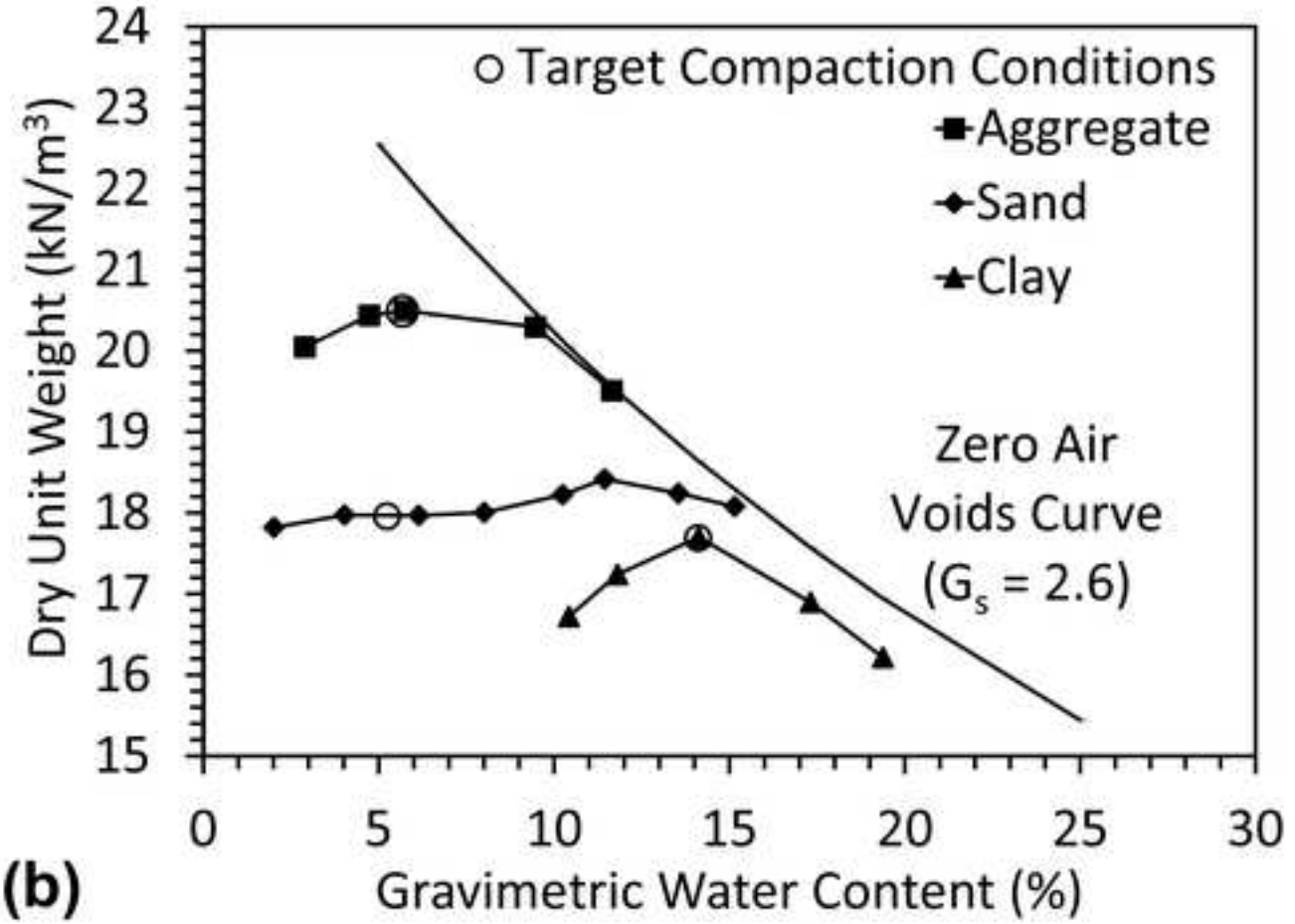


(b)

Figure 2



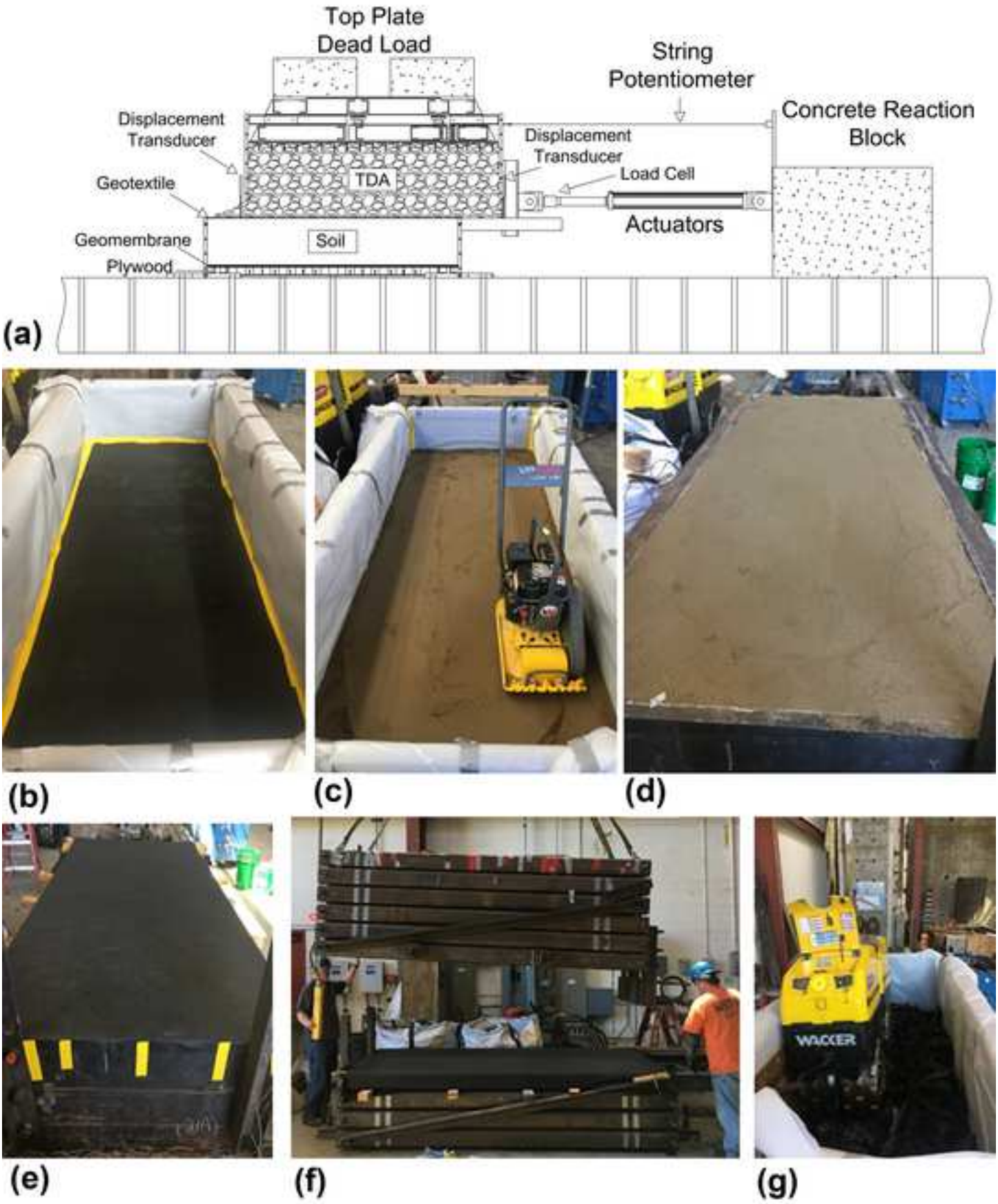

(a)

(b)

Figure 4



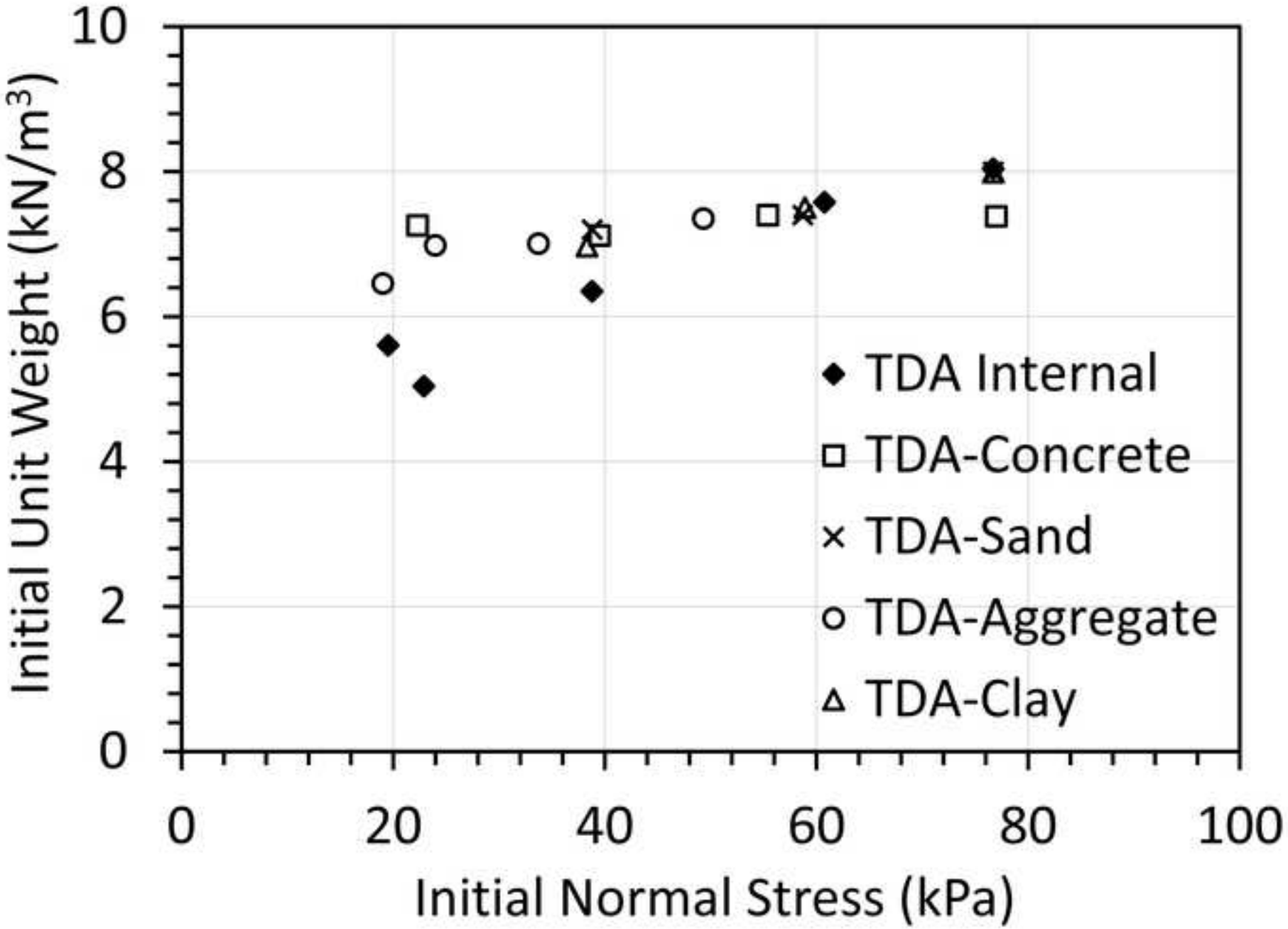

Figure 5



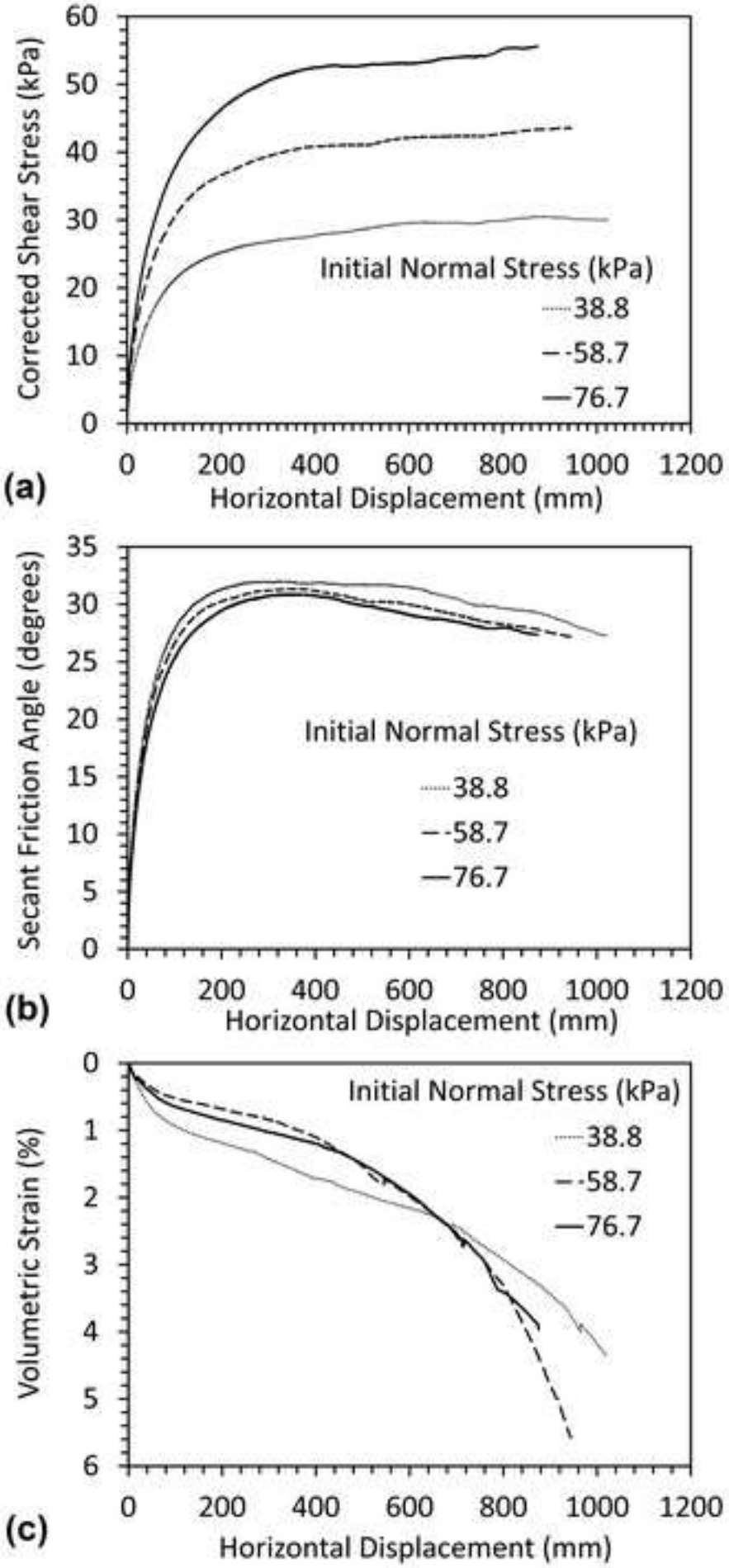

Figure 6



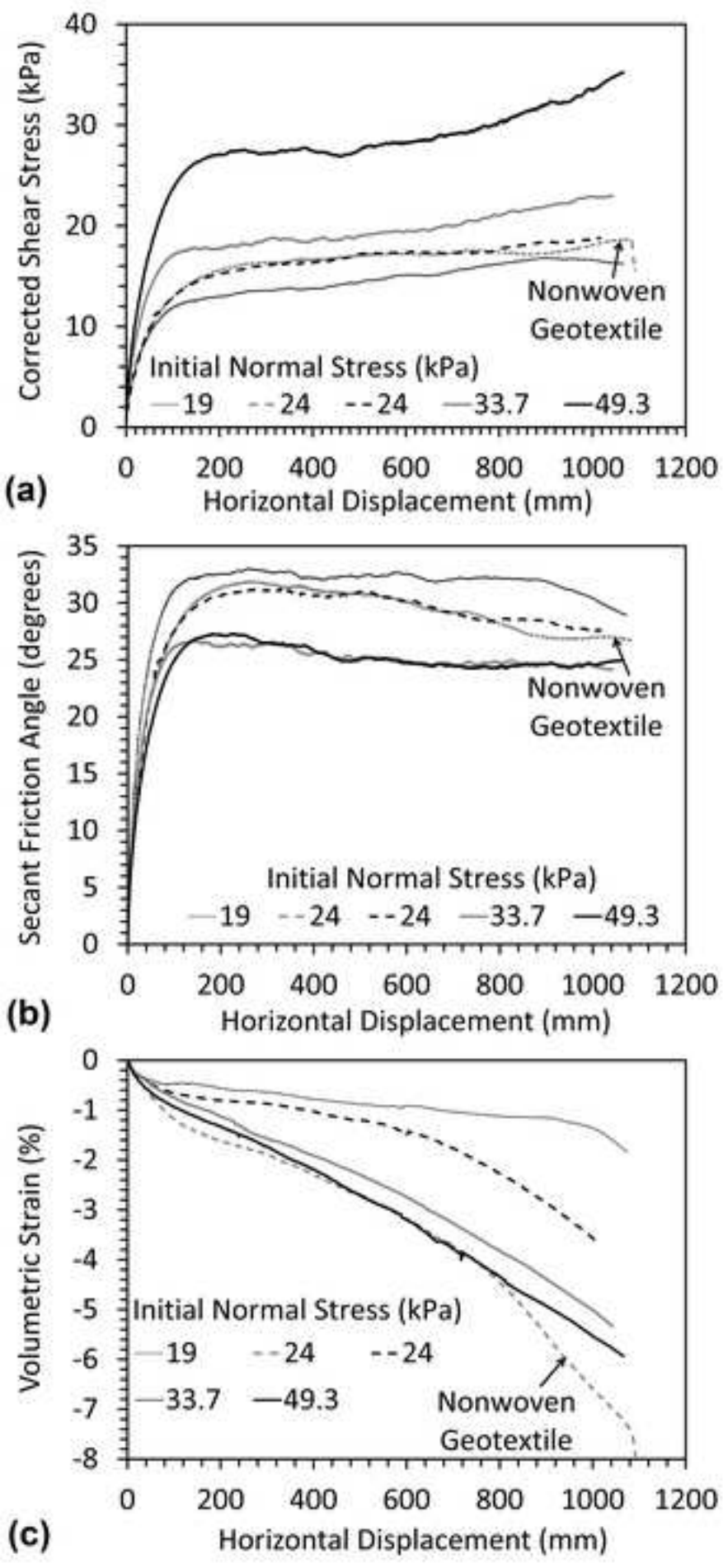

Figure 7



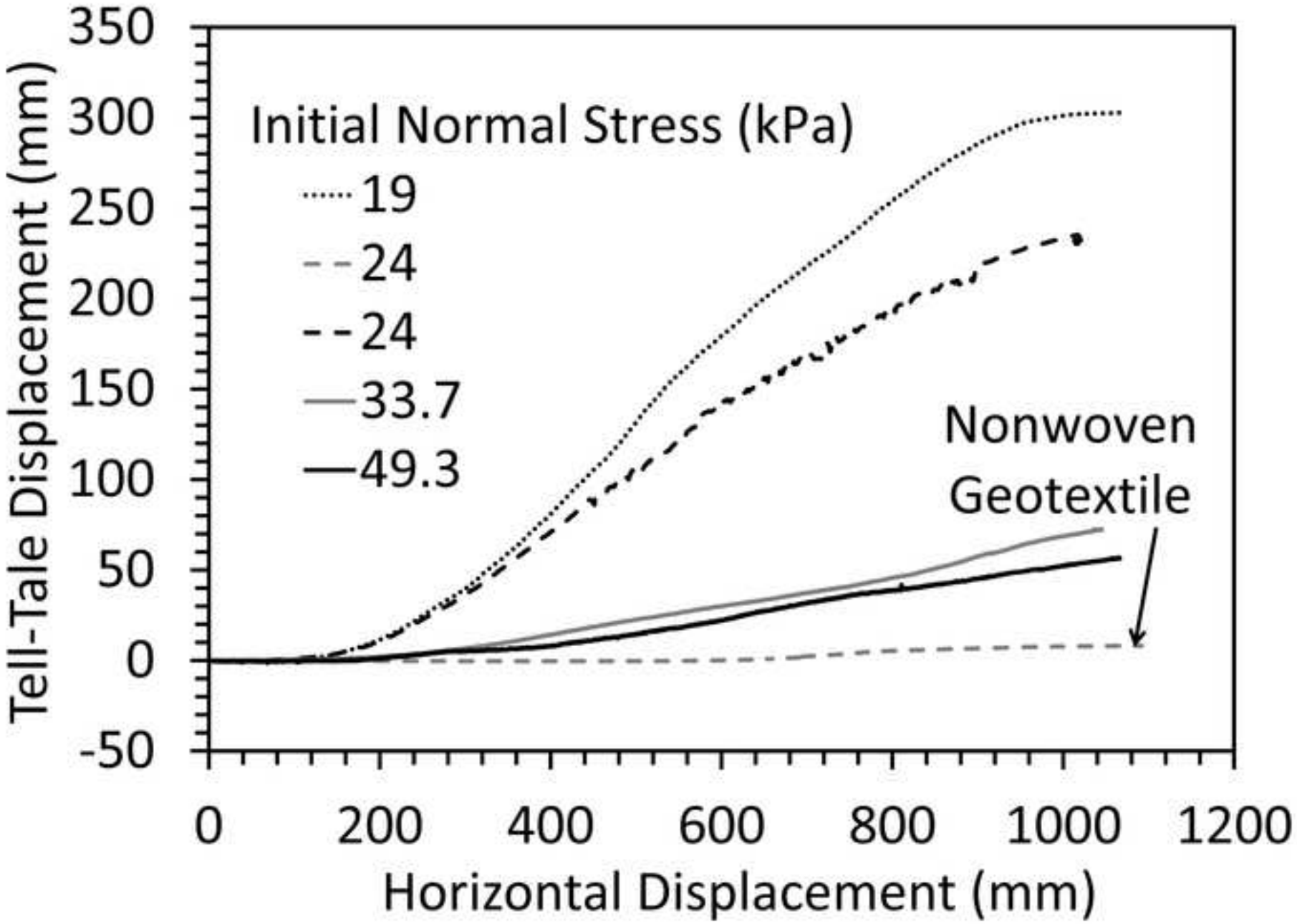

Figure 8



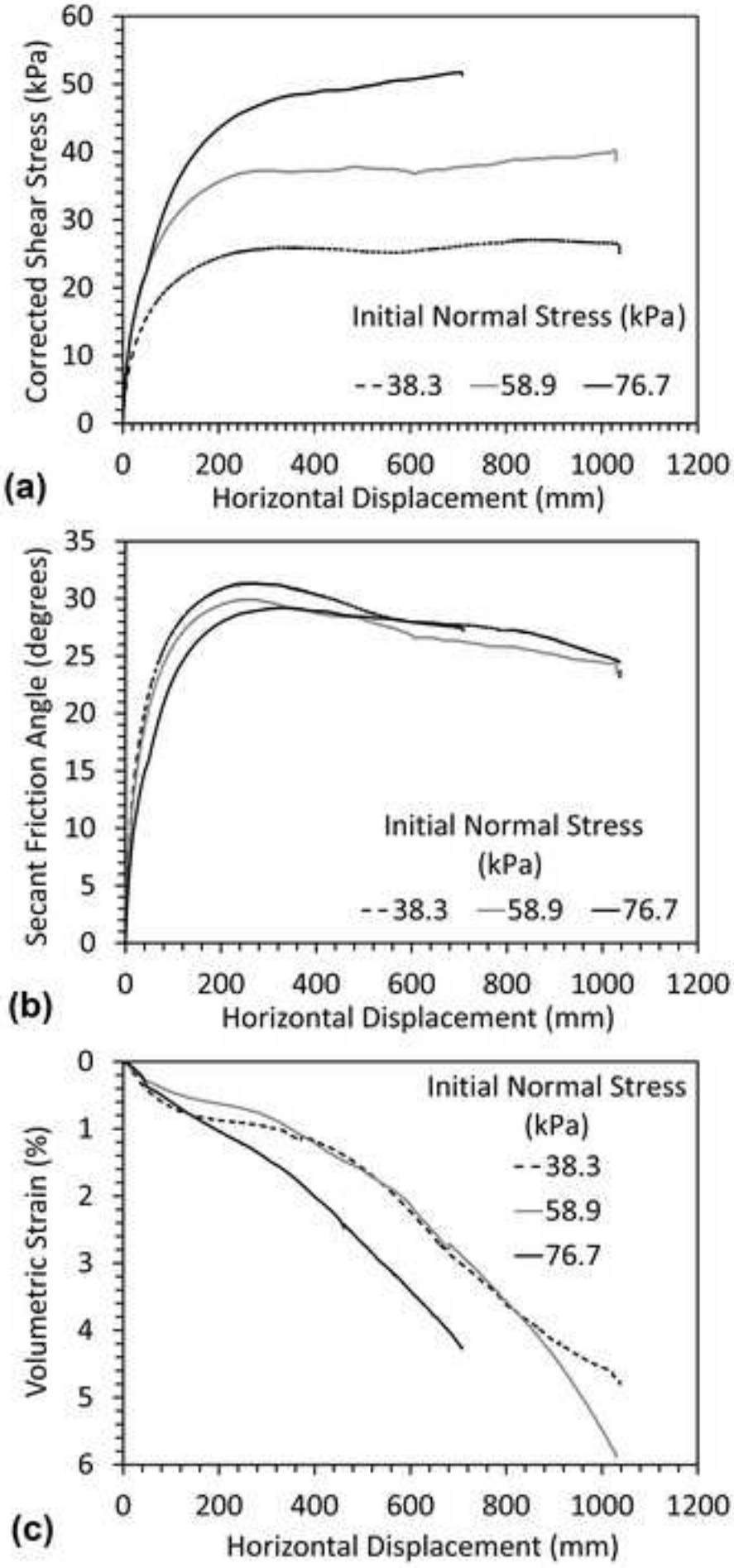

Figure 9



Figure 10

Click here to access/download;Figure;Figure 10.tif